The b Matrix in Diffusion Tensor Echo-Planar Imaging

James Mattiello, Peter J. Basser, Denis Le Bihan

In diffusion tensor imaging (DTI) an effective diffusion tensor in each voxel is measured by using a set of diffusion-weighted images (DWIs) in which diffusion gradients are applied in a multiplicity of oblique directions. However, to estimate the diffusion tensor accurately, one must account for the effects of all imaging and diffusion gradient pulses on each signal echo, which are embodied in the b matrix. For DTI to be practical clinically, one must also acquire DWIs rapidly and free of motion artifacts, which is now possible with diffusion-weighted echo-planar imaging (DW-EPI). An analytical expression for the b matrix of a general DW-EPI pulse sequence is presented and then validated experimentally by measuring the diffusion tensor in an isotropic phantom whose diffusivity is already known. The b matrix is written in a convenient tabular form as a sum of individual pair-wise contributions arising from gradient pulses applied along parallel and perpendicular directions. While the contributions from readout and phase-encode gradient pulse trains are predicted to have a negligible effect on the echo, the contributions from other imaging and diffusion gradient pulses applied in both parallel and orthogonal directions are shown to be significant in our sequence. In general, one must understand and account for the multiplicity of interactions between gradient pulses and the echo signal to ensure that diffusion tensor imaging is quantitative.

Key words: MRI; b matrix; EPI; diffusion tensor.

INTRODUCTION

MR diffusion imaging (DI) (1–3) is a noninvasive *in vivo* method to measure molecular diffusion of water in tissues, which has generated great scientific and clinical interest (4). Diffusion imaging (DI) consists of obtaining diffusion-weighted images (DWI) directly or using them to calculate an apparent scalar diffusion constant (ADC) whose value can be displayed in each voxel (5–7). However, in anisotropic tissues, such as white matter (8) and skeletal muscle (9), the scalar ADC depends on the direction of diffusion sensitizing gradient and the tissue's local fiber-tract direction. In these heterogeneous, anisotropic tissues, it is appropriate to characterize diffusive transport of water by an effective diffusion tensor, *D*, rather than an ADC (10–14).

The practical importance of the effective diffusion tensor is that it contains new and useful structural and physiological information about tissues that was previously unobtainable. Examples include the local fiber-tract direction field, the principal diffusivities, and diffusion ellipsoids, which depict the mean-squared diffusion distances of protons (15). Moreover, one can derive from *D* quantitative, scalar MR parameters that behave like histological or physiological stains (16). These include measures of mean diffusivity (or Trace(*D*)), of diffusion anisotropy of fiber structure, and of fiber organization (16), all of which are rotationally and translationally invariant, and thus are independent of fiber orientation (i.e., free of orientational artifacts) (15, 16).

Recently, we presented methods to estimate *D* from a series of diffusion-weighted spin-echo spectra (17) and subsequently, from two-dimensional Fourier transformed (2DFT) spin-echo images (18). Just as in diffusion imaging, where one estimates an apparent diffusion constant (ADC) from DWIs by using a (scalar) b factor derived from each gradient pulse sequence (19), in diffusion tensor imaging (DTI), we estimate an effective diffusion tensor (with six independent elements) from DWIs by using a b matrix (with six independent elements) derived from each pulse gradient sequence (20). Until recently, DWIs obtained by using 2DFT spin-echo sequences suffered from long acquisition times, poor spatial resolution, and high susceptibility to motion artifacts, all of which impaired the quality *in vivo* DTI and impeded its clinical implementation. However, diffusion-weighted echo-planar imaging (DW-EPI) overcomes some of these limitations (21). With it, one can acquire a diffusion-weighted image in milliseconds, without bulk motion artifacts (22–24).

Previously, we presented an analytical expression for the b matrix of a 2DFT spin-echo DW pulse sequence (18). Here we present the b matrix for a DW-EPI sequence in a more convenient tabular form. The DW-EPI sequence presents a more formidable challenge due to its multiplicity and variety of applied gradient pulses. In particular, the multiple phase-encode and read-out gradient pulses (applied during the collection of the echoes) could have a significant effect on the measured signal attenuation. By using pulse parameters appropriate for our experiment, we also calculate numerical expressions for the b matrix for the measured DWIs. We use them both to estimate (statistically) an effective diffusion tensor of water in each voxel of an isotropic phantom, from which we construct images of diffusion tensor elements, as well as diffusion ellipsoids (15) in each voxel to demonstrate the validity of this DTI protocol.

THEORY

The b Matrix of a General DW-EPI Sequence

In DI, one estimates a scalar apparent diffusion coefficient (ADC) from the measured spin-echo intensity,

$A(\tilde{b})$, using

$$\ln\left(\frac{A(\tilde{b})}{A(0)}\right) = -\tilde{b}\,\text{ADC} \qquad [1]$$

Above, $\tilde{b}$ is a scalar that depends on the pulse sequence, and $A(0)$ is the signal intensity with $\tilde{b} = 0$.

Analogously, in DTI we estimate the effective diffusion tensor, D, from the measured spin-echo, using (20):

$$\ln\left(\frac{A(b)}{A(0)}\right) = -\sum_{i=1}^{3}\sum_{j=1}^{3} b_{ij}D_{ij} \qquad [2]$$

Above, b_{ij} is a component of the symmetric b matrix, b; D_{ij} is a component of the symmetric effective diffusion tensor, D; $A(b)$ is the echo intensity for a gradient sequence whose b matrix is b, and $A(0)$ is the echo intensity for $b = 0$. The b matrix in Eq. [2] is calculated from the pulsed gradient sequence using (20):

$$b = \int_{0}^{2\tau} (\mathbf{k}(t) - 2H(t - \tau)\mathbf{k}(\tau))(\mathbf{k}(t) - 2H(t - \tau)\mathbf{k}(\tau))^{T}dt$$

[3a]

where

$$\mathbf{k}(t) = \gamma\int_{0}^{t} \mathbf{G}(t')dt';$$

[3b]

$$\mathbf{G}(t) = (G_x(t), G_y(t), G_z(t))T; \mathbf{k}(2\tau) = \mathbf{0}$$

Above, γ is the gyromagnetic ratio, 2τ is the echo time, $H(t)$ is the (Heaviside) unit-step function, and $\mathbf{G}(t)$ is the column vector representing the DWI gradient pulse sequence. Sequence parameters are always chosen so that the net phase accumulation vanishes in each direction (as in Eq. [3b]).

From Eq. [2], we see that the logarithm of the echo attenuation equals the sum of elements of the diffusion tensor, each of which is premultiplied by a corresponding element of the b matrix. Therefore, for each DWI, the b matrix provides the weights for each element of diffusion tensor that determine their contribution to the echo attenuation.

While for a diffusion tensor spectroscopic sequence one can easily derive analytical expressions for the b matrix by integrating Eq. [3] (20), for diffusion tensor imaging sequences, particularly for DW-EPI sequences, this approach is infeasible. Moreover, in DTI, one usually obtains many DWIs with different diffusion gradient strengths and directions. A new b matrix must be calculated for each DWI. Therefore, it is prudent to evaluate Eq. [3] either symbolically (as Price and Kuchel did for spectroscopic sequences (25), or as we did for 2DFT spin echo DW imaging sequences (18)), or numerically.

In calculating an analytical expression for the b matrix for the spin-echo DW-EPI sequence shown in Fig. 1, we have accounted for all gradient pulses that typically arise, including localization, crusher, and diffusion gradients; all of which are known to affect echo intensity (19, 26, 27). While the preparation period of an EPI pulse

sequence is similar to that of a 2DFT spin-echo pulse sequence, the image period of the former consists of a train of read-out and phase-encode gradient pulses. The signal generated by an EPI sequence consists of a series of echoes, each occurring at the center of its corresponding read-out gradient. In the read direction, spins are completely refocused during the first read-out gradient pulse, as in the 2DFT spin-echo pulse sequence. In the read and slice directions, the b matrix contributions of the preparation (b_{prep}) and imaging (b_{im}) periods to the b matrix may be added, ($b = b_{\text{prep}} + b_{\text{im}}$), as illustrated in Fig. 1. This additivity does not apply to the phase-encode direction, however, since spins remain out of focus at the end of the preparation period.

A commonly used approximation is to calculate the b matrix at the center of the k-space. This is partially guaranteed by the constraint that we impose when we design the DW-EPI sequence, (i.e., $\mathbf{k}(2\tau) = \mathbf{0}$). Strictly, since the b matrix depends on all gradient pulses "seen" by the spins at a given time t, each point of k-space should be associated with a specific b matrix:

$$A(\mathbf{r}) = \int\int\int \tilde{A}(\mathbf{k})\exp(i\mathbf{k}\cdot\mathbf{r})\exp\left(-\sum_{i=1}^{3}\sum_{j=1}^{3} b_{ij}(\mathbf{k})D_{ij}(\mathbf{r})\right)d\mathbf{k} \quad [4]$$

where $\mathbf{r}$ is the position vector, and $\tilde{A}(\mathbf{k})$ is the signal with T_1, T_2, and proton density contribution. Considering that diffusion contrast is given by low spatial frequencies, the b matrix is usually calculated at the center of the k-space, so Eq. [4] is approximated by:

$$A(\mathbf{r}) \approx \exp\left(-\sum_{i=1}^{3}\sum_{j=1}^{3} b_{ij}(\mathbf{0})D_{ij}(\mathbf{r})\right)\int\int\int \tilde{A}(\mathbf{k})\exp(i\mathbf{k}\cdot\mathbf{r})d\mathbf{k}$$

[5]

In the case of a conventional 2D-FT spin-echo pulse sequence, this means that we can calculate the b matrix without considering the phase-encoding gradient at the top of the echo. However, in EPI this is no longer possible, since multiple phase-encode gradient pulses are dispersed throughout the readout period. Furthermore, the large number of large amplitude, short duration read-out gradient pulses that occur during the collection of the echoes could introduce cumulative errors into the calculation of the b matrix if only the center of k-space were used.

CALCULATING THE ELEMENTS OF THE *b* MATRIX

In obtaining an analytical expression for the b matrix from Eq. [3], we synthesized a generalized DW-EPI gradient pulse sequence, $\mathbf{G}(t)$, shown in Fig. 1, from a library of sinusoidal and trapezoidal pulses, and integrated them by using *Mathematica*. The parameter values for each sequence are given in the caption of Table 1. By specifying the plane of the image to be acquired, we also specify the read, phase, and slice directions with respect to x-, y-, and z laboratory frame. It is generally more convenient to express the b matrix elements in the coordinate frame of

the image rather than in the laboratory frame. Therefore, we use the subscripts r, s, and p, corresponding to "read-out," "slice-select," and "phase-encode," rather than the subscripts x, y, and z. However, it is always straightforward to transform between the image coordinate system and the laboratory coordinate system.

EXPERIMENTAL METHODS

From the analytical expressions in Eqs. [6]–[11], we calculated the diagonal and off-diagonal elements of the b matrix each measured by using parameters derived from an EPI pulse sequence that was originally proposed by Turner et al. for diffusion imaging (6, 7), but which we adapted to diffusion tensor imaging. We acquired coronal DWIs (64×64 pixels) of a water phantom in a glass sphere whose temperature was stable at 15°C during image acquisition. Trapezoidal diffusion gradients were applied in seven non-collinear (oblique) directions (read, phase, slice, read and phase, phase and slice, read and slice, and read and phase and slice).[1] We acquired a total of 112 images on a 4.7-T spectroscopy/imaging system (GE Omega, Fremont, CA). The diffusion gradients were incremented in 16 equal steps from 0 to 1.5 G/mm (150 mT/m). The b matrix for each image was calculated off-line by using the imaging and diffusion gradient parameters calculated from an EPI pulse sequence listed in Table 2.

Our imaging parameters were as follows: phase-encode resolution (res) = 64, slice thickness = 2 mm, ramp time (rt) = 0.500 ms, read-out ramp time (rtr) = 0.200 ms, echo time ($2\tau = TE$) = 85.710 ms, and repetition time (TR) = 15 s. The ramp time for the read-out and phase-encode gradients can be different from the ramp time for the other imaging gradients.

Once numerical values of the b matrix were calculated from the analytical expressions for each DWI, we used multivariate linear regression of Eq. [2], as described in ref. 20, to estimate D in each voxel from the series of DWIs.

RESULTS AND DISCUSSION
Analytical Expressions for the b Matrix

Equation [5] allows us to determine analytical expressions for the diagonal and off-diagonal elements of the b matrix for the DW-EPI pulse sequence shown in Fig. 1. The evaluation of the b matrix is greatly simplified by observing that the complicated double integral in Eq. [3] can be expressed as a sum of pair-wise interactions between individual gradient pulses (18) whose terms represent the product of two gradient amplitudes (G^2/mm^2) and a timing parameter (s^3). For a DW-EPI sequence, some of these interactions are illustrated in Fig. 1 and explained in detail in its caption. The analytical expressions for the b matrix represent the sum of contributions arising from individual pair-wise interactions between
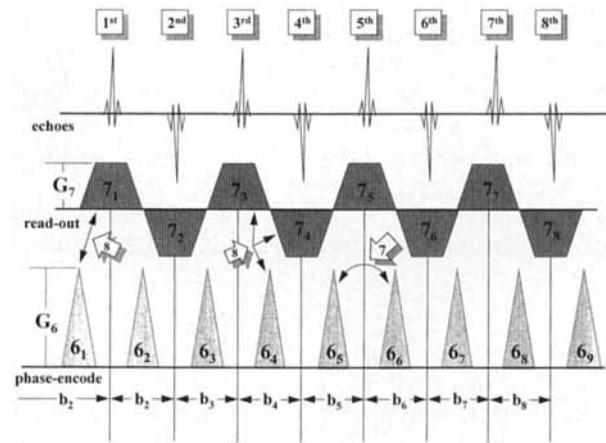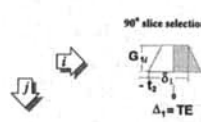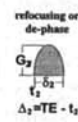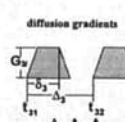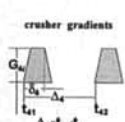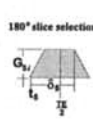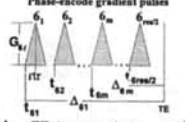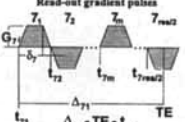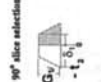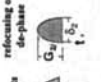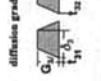

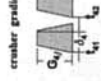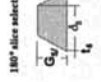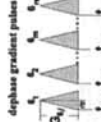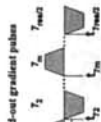FIG. 1. A general (DW-EPI) sequence. The imaging and diffusion gradient intensities are as follows: G_1 is a 90° slice-selection gradient; G_2 is a read-dephasing, phase-dephasing, or slice-refocusing gradient; G_3 is a diffusion gradient in the read, phase, or slice directions, respectively; G_4 are the crusher gradients in the read, phase, or slice directions, respectively; G_5 is the 180° slice-selection gradient; G_6 is the phase-encode gradient train; and G_7 is the read-out gradient train. The numbered boxes indicate pairwise interactions that may exist between gradients in a typical DW-EPI pulse sequence. They are between: 1) diffusion gradients in the same direction (i.e., read and read, phase and phase, or slice and slice); 2) diffusion gradients in different directions (i.e., read and phase, read and slice, or phase and slice); 3) diffusion gradients and imaging in the same direction (e.g., read-dephase and read diffusion gradients, or 90° slice selection gradients and slice diffusion gradients); 4) diffusion gradients and imaging in different (orthogonal) directions (e.g., read-dephase and slice diffusion gradients, or phase crusher gradients and slice diffusion gradients); 5) imaging gradients in the same direction (e.g., between a pair of read crusher gradients, a 90° slice refocusing gradient and 90° slice selection gradient, or a read-dephase gradient and read-out gradients); 6) imaging gradients in different (orthogonal) directions (e.g., read crusher gradients and slice crusher gradients, read-dephase gradient and 180° slice selection gradient); 7) a series of imaging gradients in the same direction (i.e., the phase-encode gradient pulses); and 8) a series of imaging gradients in different (orthogonal) directions (i.e., read-out and phase-encode gradients). Only the interactions labeled 1, 3, and 5 had been considered previously in diffusion imaging.

individual gradient pulses in $\mathbf{G}(t)$ (i.e., those in which most other gradients are set to zero). In this way, we are able to construct a table of all the possible interactions between one gradient pulse and all other relevant gradient pulses occurring in the sequence, given in Table 1. Moreover, to evaluate any b matrix element, one simply sums up the appropriate elements of Table 1. The form of Table 1 illustrates the fact that the b matrix can be expressed as a sum of terms each of which represents an individual pair-wise interaction between imaging or diffusion gradient pulses applied along the same or along orthogonal directions (18).

Recognizing that the b matrix is a sum of pair-wise interactions between gradient pulses also greatly simplifies the process of evaluating the b matrix for a new or modified imaging sequence. Once we have calculated the contribution of one gradient pair (for example, between two trapezoidal diffusion or crusher gradients), we do not have to recalculate them when we modify an existing

---

[1] Technically, it is only necessary to apply diffusion gradients in six non-collinear directions.

Table 1
The Analytical Expression for b_{ij} and a Pictoral Representation of How Each of Its Terms Arise

This table shows all possible pair-wise interactions between pulsed gradients in the general DW-EPI sequence shown in Fig. 1. All the gradient magnitudes and timing parameters are illustrated in cartoons of the gradient pulses. The top row indicates the gradient pulses that may be present in one gradient sequence, $G_i(t)$; the far-left column indicates the gradient pulses that may be present in another gradient sequence, $G_j(t)$. To use this table to calculate the *b* matrix for each sequence, identify all those pulses that do not appear in the sequence and set their gradient magnitudes to zero, then just add the remaining terms in the table to obtain the *b* matrix element $b_{ij} = b_{ji}$.

sequence or analyze a new sequence. Therefore, many of the terms that we have already derived for the 2DFT spin echo DW imaging sequence also appear in the b-matrix of the DW-EPI sequence (18).

Sometimes, by inspection or design (e.g., by exploiting symmetry principles), one can further simplify the form of the *b* matrix. First, interactions between a refocused pulse and pulses applied previously or subsequently in orthogonal directions do not contribute to the off-diagonal elements of *b*. For example, the 180° slice-select gradient, as well as the diffusion and crusher gradient pairs applied in the slice-selection direction are effectively refocused in the spin echo sequence, and therefore produce no pair-wise interactions with the readout and phase-encode gradient pulse trains. Analytically, this is because the integrals of $k_s(t) k_p(t)$ as well as $k_s(t) k_r(t)$ (in Eq. [3]) are unchanged by the application of these refocused pulses. In Table 1, these interactions contribute zero to the *b* matrix. In addition, the potentially complex interactions between read-out and phase-encode gradient pulse trains in the EPI sequence can be shown to have no effect on b_{rp} during each of the periods b2 through b8 in

Fig. 2. During each of these periods, owing to the (odd and even) symmetry of these pulses there is no net contribution to the integral of $k_r(t) k_p(t)$ (in Eq. [3]). Therefore, only the first half of the first readout gradient pulse (G_{71}) and of the first phase-encode gradient (G_{61}) contribute to the *b* matrix element b_{rp}. In general, one can mitigate (and sometimes eliminate) the contribution of any imaging gradient to the *b* matrix by refocusing it as soon as possible after it is applied. Clever pulse sequence design strategies that simplify the form of the *b* matrix are strongly recommended and encouraged.

Using Table 1 to Evaluate the b Matrix

Figure 1 contains a DW-EPI sequence for which a general *b* matrix is calculated using Eq. [3]. Since each element of this general *b* matrix is a sum of pair-wise interactions between applied gradients, evaluating it just requires identifying which pair-wise interactions to retain and which to ignore. In Table 1, the G_{ki} represent the pulse gradient magnitudes. The first index, k, indicates the type of gradient pulse (e.g., slice-selection, phase-en-
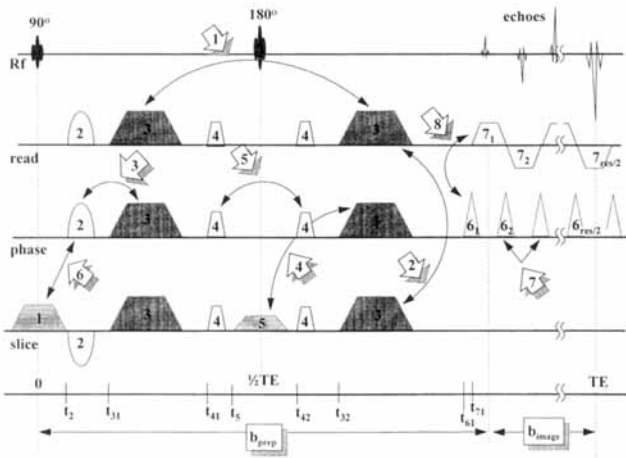
FIG. 2. The phase-encode and read-out gradient pulse train for a series of eight echoes. To calculate the b matrix elements b_{rr} and b_{pp}, we integrated up to the center of k-space (top of the echo) for each read-out and phase-encode gradient, respectively. We see that, by symmetry, contributions to b_{rp} from periods $b2$ through $b8$ vanish.

code, etc.). The imaging and diffusion gradient intensities are defined as follows: $k = 1$ corresponds to a 90° slice-selection gradient; $k = 2$ corresponds to the read-dephasing, phase-dephasing, or slice-refocusing gradients, respectively; $k = 3$ corresponds to the diffusion gradients in the read, phase, and slice directions, respectively; $k = 4$ corresponds to the crusher gradients in the read, phase, and slice directions, respectively; $k = 5$ corresponds to the 180° slice-selection gradient; $k = 6$ corresponds to the phase-encode gradient train; and $k = 7$ corresponds to the read-out gradient train. The second index, i, indicates the coordinate direction in which that pulse is applied (i.e., the read, phase, or slice direction); the index m indicates the gradient number (i.e., 1st, 2nd, 3rd, . . .). For gradient pulses lying along the same coordinate direction, $i = j$; for gradient pulses lying along different coordinate directions, $i \neq j$.

To determine the component b_{ij}, we first inspect the gradient sequences $G_i(t)$ and $G_j(t)$ (e.g., in Fig. 1). Then we identify all pulses present in $G_i(t)$ depicted along the top row of Table 1, and all pulses present in $G_j(t)$ depicted along the left column. All pulses shown in Table 1 that do not appear in $G_i(t)$ can be eliminated either by drawing a vertical line through them that extends down the column or by setting their gradient magnitudes to zero. All pulses depicted in Table 1 not appearing in $G_j(t)$ can similarly be eliminated either by drawing a horizontal line through them that extends across a row or by setting their gradient magnitudes to zero. Now that all gradient pulses have been accounted for, the b matrix element, b_{ij} is then obtained by taking the sum of all the remaining elements given in Table 1. By performing these steps for each pair of gradient sequences, we can determine each element of the b matrix.

For instance, when we insert the pulse parameters given in Table 2 and in the Methods section in the expressions for the components of the b matrix elements given in Table 1, we obtain the following numerical expressions:

$$b_{rr} = 3.51 + 136.89G_{3r} + 2228.52G_{3r}^2 \tag{6a}$$

$$b_{pp} = 3.19 + 130.63G_{3p} + 2228.52G_{3p}^2 \tag{6b}$$

$$b_{ss} = 1.76 - 58.50G_{3s} + 2228.52G_{3s}^2 \tag{6c}$$

$$b_{rp} = b_{pr} = 3.17 + 68.45G_{3p} + 65.31G_{3r} \\ + 2228.52G_{3r}G_{3p} \tag{6d}$$

$$b_{ps} = b_{sp} = -1.84 - 29.25G_{3p} + 65.31G_{3s} \\ + 2228.52G_{3p}G_{3s} \tag{6e}$$

$$b_{rs} = b_{sr} = -1.93 - 29.25G_{3r} + 68.45G_{3s} \\ + 2228.52G_{3r}G_{3s} \tag{6f}$$

Table 2
Parameters for a 4.7 T MR System

i	δ_i ms	t_i ms	G_i	G/mm
1	2.2500	−1.3750	Gs1	−0.281
2	2.0000	1.3750	Grdp	0.129
			Gpdp	0.123
			Gsrf	0.248
3			Gdr	0 to 0.994
(31)	10.5000	21.480	Gdp	0 to 0.951
			Gds	0 to −0.948
4			Gcr	0.201
(41)	2.5000	37.480	Gcp	0.192
			Gcs	−0.191
5	2.2500	41.480		
(42)		45.230		
(32)		53.230		
61	0.2000	65.230	Gpe	0.0244
71	0.4400	65.430	Gro	0.489

The parameters used to calculate b matrix values for a DW-EPI pulse sequence, including the gradient strength and timing parameters used to calculate the b matrix values for the DW-EPI pulse sequence shown in Fig. 1. The kth gradient pulse strengths (G_k), the gradient pulse timing parameter (δ_k), and the time during which the gradient pulses are turned on during the pulse sequences (t_k) are also defined.

These expressions show how the b matrix elements (given in (s/mm^2)) depend on the diffusion gradient strengths, G_{3r}, G_{3p}, and G_{3s} (G/mm) in our experiment. In DTI we acquire a series of DWIs by varying the strength and sign of the three diffusion gradients from which we obtain estimates of D (20). (Above, G_{3s} is assumed to be negative; see Table 2). In Eqs. [6a]–[6f], all constant terms arise solely from interactions between imaging gradients. All linear terms in G_{3r}, G_{3p}, or G_{3s} arise solely from interactions between imaging and diffusion gradients. Finally, all quadratic terms in G_{3r}, G_{3p}, or G_{3s} arise solely from interactions between diffusion gradients. The diagonal elements of the b matrix (i.e., b_{pp}, b_{ss}, b_{rr}) contain contributions from interactions between gradient pulses applied along the same direction, whereas the off-diagonal elements of the b matrix (i.e., b_{rp}, b_{ps}, b_{rs}) contain contributions from interactions between gradient pulses applied along orthogonal directions. The terms that are quadratic in only one of the diffusion gradients (i.e., G_{3r}^2, G_{3p}^2, and G_{3s}^2) result from interactions between diffusion gradients applied along the same direction. These are the well-known "Stejskal and Tanner" terms used in diffusion spectroscopy and (by many) in diffusion imaging to estimate ADCs. The other quadratic terms (i.e., $G_{3r}G_{3p}$, $G_{3p}G_{3s}$, and $G_{3r}G3s$) represent interactions between diffusion gradients applied in *orthogonal* directions (20). We consider all terms in Eqs. [6a]–[6f] that do not depend on products of diffusion gradients, (i.e., are not of the form $G_{3i}G_{3j}$ "cross terms" because they depend on imaging gradients. While the effect that gradients applied in the same directions have on the echo magnitude had previously been considered in diffusion imaging studies (19, 26, 27), the effect that gradients applied in orthogonal directions have on the echo magnitude had not until recently (18, 20). Some of the pairwise interactions between gradients pulses that give rise to cross terms are illustrated in Fig. 1. In summary, diffusion tensor imaging provides a more general framework than diffusion imaging for treating the contribution that each gradient pulse has on echo attenuation in diffusion weighted sequences.

To assess the importance of the applied diffusion gradients, b-matrices below were calculated using Eqs. [6a]–[6f]. When no diffusion gradients are applied (i.e., $G_{3r} = G_{3p} = G_{3s} = 0.0$ G/mm), the b matrix $b(G_{3r}, G_{3p}, G_{3s})$, written as a function of diffusion gradient amplitudes, becomes,

$$b(0.0, 0.0, 0.0) = \begin{pmatrix} 3.51 & 3.16 & -1.93 \\ 3.16 & 3.19 & -1.84 \\ -1.93 & -1.84 & 1.76 \end{pmatrix} (\text{s/mm}^2) \quad [7]$$

When $G_{3r} = 0.2$ G/mm, the b-matrix becomes:

$$b(0.2, 0.0, 0.0) = \begin{pmatrix} 120.03 & 16.23 & -7.78 \\ 16.23 & 3.19 & -1.84 \\ -7.78 & -1.84 & 1.76 \end{pmatrix} (\text{s/mm}^2) \quad [8]$$

When $G_{3r} = G_{3s} = 0.2$ G/mm, the b matrix becomes:

$$b(0.2, 0.0, 0.2) = \begin{pmatrix} 120.03 & 16.23 & 95.05 \\ 16.23 & 3.19 & -7.69 \\ 95.05 & -7.69 & 79.2 \end{pmatrix} (\text{s/mm}^2) \quad [9]$$

Similarly, when $G_{3r} = G_{3p} = G_{3s} = 0.2$ G/mm, then the b matrix becomes:

$$b(0.2, 0.2, 0.2) = \begin{pmatrix} 120.03 & 119.06 & 95.05 \\ 119.06 & 118.45 & 94.51 \\ 95.05 & 94.51 & 79.2 \end{pmatrix} (\text{s/mm}^2) \quad [10]$$

Eqs. [7]–[10] represent a typical range of b matrix values for a clinical EPI system. If we recall that the b matrix elements are weighting factors calculated for each DWI that are used to estimate the diffusion tensor elements, then we can appreciate the enormous range of relative weights of different elements of the diffusion tensor can be subjected to (both diagonal and off-diagonal elements).

By inspecting Eqs. [6]–[10], we see that cross-terms are significant in this DWI sequence. For example, in Eq. [8] where diffusion gradients are applied only in the "r" direction, one might expect that all b matrix elements other than b_{rr} would vanish. Yet all other elements of the b matrix are non-zero, and two are as high as 10% of b_{rr}. We can assess the significance of cross-terms in this DW-EPI sequence by evaluating the error made in estimating the effective diffusion tensor when we ignore them. Figure 3 shows the fractional error in b_{rr}, $\Delta b_{rr}/b_{rr}$, that was calculated from Eq. [6a] plotted against applied
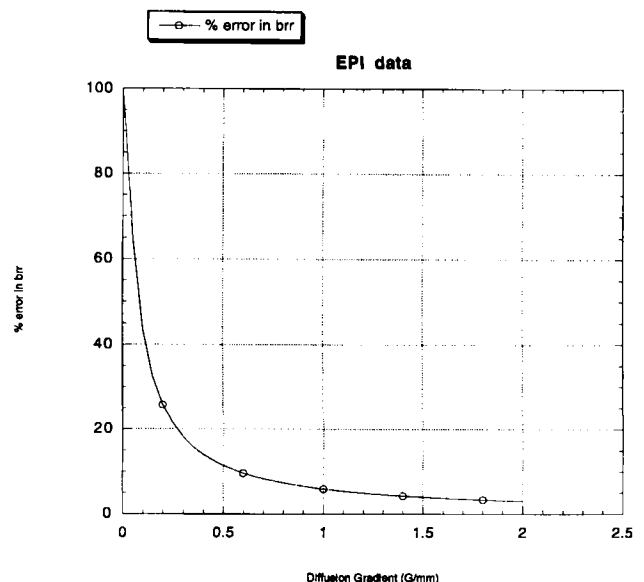

FIG. 3. The fractional error in b_{rr}, $\Delta b_{rr}/b_{rr}$ (from Eq. [6a]), plotted against the applied diffusion gradient strength, *Gdr*. When *Gdr* = 0, the percentage error in b_{rr} is 100%. The error drops off to about 20% for *Gdr* = 0.2 G/mm, which is typical for the peak gradient strength in a clinical EPI system, and is still about 5% for *Gdr* = 2.0 G/mm.

diffusion gradient strength, G_{3r}. When $G_{3r} = 0$, the percentage error in b_{rr} is 100%. The error drops off to about 20% for $G_{3r} = 0.2$ G/mm (a typical peak gradient strength for a clinical EPI system) and to about 5% for $G_{3r} = 2.0$ G/mm! Since we can easily show from Eq. [2] that the percentage error in b_{ij} equals the percentage error in the estimated D_{ij}, we can see immediately that omitting the effect of imaging gradients on the echo attenuation produces a significant error in the estimated diffusion tensor.

However, ignoring cross terms introduces additional deleterious errors. Even when a diffusion gradient is applied only along one direction, all diagonal and off-diagonal elements of the b matrix are still significantly different from zero. Above, we see this is true when the diffusion gradient is zero (as in Eq. [7]) or is large (as in Eq. [8]). This means that each element of D potentially can contribute to the observed signal attenuation. However, when one uses the scalar model of diffusive transport (Eq. [1]) rather than the tensor model (Eq. [2]), one tacitly assumes that the signal attenuation results entirely from the action of gradients applied in the direction in which the diffusion gradient is applied.

The Importance of Imaging Gradients in DW-EPI

Avram and Cooks (5) and Turner and LeBihan (6) suggested that the read-out gradients in the imaging phase of the EPI pulse sequence have a negligible effect on the signal attenuation due to diffusion. We can assess this assertion quantitatively by using the imaging sequence shown in Fig. 1, the imaging parameters given in Table 2, and the b matrix formulae given in Eqs. [6a]–[6f]. In the read direction, the contribution to the b matrix during the image period is $b_{rr(im)} = 0.082$ s/mm², which is negligible. But if we treat each read-out gradient separately, we see that the read-out gradient train provides a small but significant contribution to b_{rr}. The effect of all readout gradients is 2.3% of b_{rr} when the diffusion gradient G_{3r} is 0.0 G/mm and 0.07% of b_{rr} when G_{3r} was 0.2 G/mm. Interestingly, because of the symmetry of the read-out and phase-encode pulses (discussed above), the interaction between these two gradient pulse trains is negligible. It is only 0.004 s/mm², which is less than 0.1% of b_{rp}.

Although individual phase-encode gradient pulses are small, their integrated effect may still be significant. In Eq. [3], the contribution to the b matrix is not simply additive because the cumulative phase shifts are then integrated a second time. Even though its contribution to b_{pp} is 0.121 s/mm², which is negligible, the contribution of the phase-dephasing gradient is not. Its contribution was 3.5% of b_{pp} when the diffusion gradient strength was 0.0 G/mm, and only 0.1% of b_{pp} when the diffusion gradient strength was 0.2 G/mm.

Validating the b Matrix

In principle, in an isotropic medium such as water, all off-diagonal elements of the diffusion tensor vanish and the three diagonal elements are equal to the scalar diffu-

sivity, D_0, i.e.,

$$D = D_0 I = D_0 \begin{pmatrix} 1 & 0 & 0 \\ 0 & 1 & 0 \\ 0 & 0 & 1 \end{pmatrix} \qquad [11]$$

where I is the identity tensor, and D_0 is the scalar self-diffusion constant at the temperature of the experiment (e.g., see ref. 20).

To validate the calculated b matrices, we estimate D of water from a series of DWIs, and then assess whether the estimated D is isotropic, (i.e., is of the form given in Eq. [11]). If our b matrix elements were calculated incorrectly, then we would expect the off-diagonal elements of D to be significantly different from zero, and the diagonal elements of D to be significantly different from each other, as well as different from D_0. This is because a given percentage error in the b matrix element produces the same percentage error in the corresponding element of the (statistically) estimated diffusion tensor element but of an opposite sign (16). Therefore, an underestimated b matrix element should produce an overestimate in the corresponding diffusion tensor element, and visa versa. Therefore, errors in b should cause errors in D, which should make the estimated D for water deviate from isotropy.

In the Methods section above, we explained how we estimate D in each voxel from a set of DW-EPIs by using the analytical expression for the b matrix that we evaluate numerically for each DWI. Figure 4 shows images of the six independent components of D for a water phantom obtained by using this method. Images of each of the three diagonal components (D_{xx}, D_{yy}, and D_{zz}) have a high but uniform intensity, while images of the three off-diagonal components (D_{xy}, D_{xz}, and D_{yz}) are all at the level of background noise, indicating they are not statistically significant. Interestingly, they also show an edge enhancement at the interface between the water sample and the glass container. This artifact is caused by local gradients produced at the water/glass interface owing to their differences in magnetic susceptibility. Susceptibil-
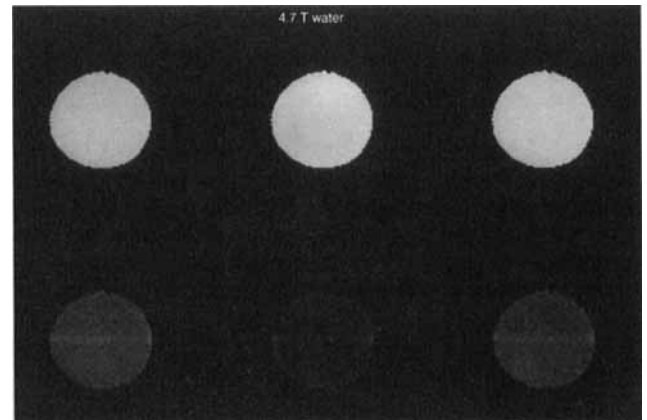

FIG. 4. Images of each of the six independent components of the estimated effective diffusion tensor, D, derived from DW-EPI for a water phantom. Top row (left to right): images of the diagonal components of D (D_{xx}, D_{yy}, and D_{zz}) bottom row (left to right): images of the off-diagonal components of D (D_{xy}, D_{xz}, and D_{yz}).

ity gradients are, of course, not explicitly accounted for in the calculation of the b matrix.

From a 16×20 pixel region of interest (ROI) in the water phantom, the mean effective diffusion tensor and its covariance were measured:

$$D = \begin{pmatrix} 1.675 \pm 0.018 & -0.011 \pm 0.007 & 0.005 \pm 0.007 \\ -0.011 \pm 0.007 & 1.680 \pm 0.014 & 0.016 \pm 0.007 \\ 0.005 \pm 0.007 & 0.016 \pm 0.007 & 1.665 \pm 0.013 \end{pmatrix}$$

$$\cdot 10^{-3} \text{ mm}^2/\text{s} \quad [12]$$

The value of the diffusion coefficient of water at $15°C$ has previously been reported as $D_0 = 1.69 \pm 0.02 \times 10^{-3}$ mm^2/s (28, 29). The diagonal elements of D that we measured in Eq. [12] compare extremely well with D_0. Moreover, the off-diagonal elements of D are negligible. D_{xz} is statistically indistinguishable from zero, while D_{xy} and D_{yz} are significantly different from zero but still negligibly small. Overall, Eq. [12] has a form consistent with that of an isotropic tensor.

To assess the degree of spatial variability or heterogeneity, as well as the degree of anisotropy of the estimated diffusion tensors in each voxel, we also constructed a diffusion ellipsoid image (see Fig. 5), as described previously (15) for the 16×20 pixel ROI. As expected from both the isotropic form of the estimated D, and the small variances reported in Eq. [12], the ellipsoids are all spherical with diameters that are uniform from voxel to voxel. Their shape and size indicate that there is no preferred direction for diffusion, and that there is virtually no variability or heterogeneity in the measured diffusion coefficient of water in the phantom, which we would have expected if we made a systematic error in accounting for imaging gradients. If the diagonal elements were not all similar, or if the off-diagonal components were significantly different from zero, these spheres then would appear as prolate ellipsoids, with their polar axes aligned. These control studies demonstrate that we have made no systematic errors in calculating the diagonal and off-diagonal elements of the b
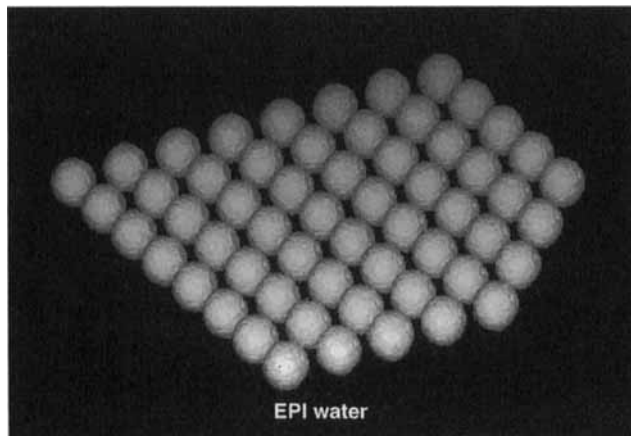

FIG. 5. Diffusion ellipsoid image. Ellipsoids are constructed in each voxel of an ROI from D estimated in each voxel whose components are shown in Fig. 4. The spherical ellipsoids are consistent with water being "isotropic", indicating that correct b matrix values were calculated.

matrix from the gradient pulse sequence, and that we estimated the effective diffusion from the measured echoes properly, as well. Performing a calibration study like this one is highly recommended before performing DTI on tissues or other media.

CONCLUSIONS

In arriving at an analytical expression for the diagonal and off-diagonal elements of the b matrix for a DW-EPI pulse sequence, we have taken into account the contributions arising from all applied imaging and diffusion gradients (i.e., applied along parallel and perpendicular directions). These analytical expressions permit one to evaluate the b matrix for a general DW-EPI sequence efficiently, off-line. They also permit one to estimate statistically the diagonal and off-diagonal elements of the effective diffusion tensor, D, accurately and efficiently from a series of DW-EPIs. This innovation has facilitated the successful implementation of high-resolution, high-quality, quantitative DTI (30), and may facilitate the development of quantitative DT-MR microscopy (e.g., ref. 31), where large imaging gradients are required to attain high spatial resolution.

ACKNOWLEDGMENTS

REFERENCES

1. D. G. Taylor, M. C. Bushell, The spatial mapping of translational diffusion coefficients by the NMR imaging technique. *Phys. Med. Biol.* **30**, 345–349 (1985).
2. K. D. Merboldt, W. Hanicke, J. Frahm, Self-diffusion NMR imaging using stimulated echoes. *J. Magn. Reson.* **64**, 479–486 (1985).
3. D. Le Bihan, E. Breton, Imagerie de diffusion in-vivo par resonance magnetique nucleaire. *Cr. Acad. Sci. (Paris)* **301**, 1109–1112 (1985).
4. D. Le Bihan, R. Turner, P. Douek, N. Patronas, Diffusion MR imaging: clinical applications. *Am. J. Roentgenol.* **159**, 591–599 (1992).
5. H. E. Avram, L. E. Cooks, in "Proc., SMRM, 7th Annual Meeting, San Francisco, 1988," p. 980.
6. R. Turner, D. LeBihan, Single shot diffusion imaging at 2.0 Tesla. *J. Magn. Reson.* **86**, 445–452 (1990).
7. R. Turner, D. Le Bihan, J. Maier, R. Vavrek, L. K. Hedges, J. Pekar, Echo-planar imaging of intravoxel incoherent motion. *Radiology* **177**, 407–414 (1990).
8. M. E. Moseley, Y. Cohen, J. Kucharczyk, J. Mintorovitch, H. S. Asgari, M. F. Wendland, J. Tsuruda, D. Norman, Diffusion-weighted MR imaging of anisotropic water diffusion in cat central nervous system. *Radiology* **176**, 439–445 (1990).
9. G. G. Cleveland, D. C. Chang, C. F. Hazlewood, H. E. Rorschach, Nuclear magnetic resonance measurement of skeletal muscle: anisotropy of the diffusion coefficient of the intracellular water. *Biophys. J.* **16**, 1043–1053 (1976).
10. S. R. DeGroot, P. Mazur, "Non-equilibrium thermodynamics," Dover Publications, New York, 1984.
11. L. Onsager, Reciprocal relations in irreversible processes. Part I. *Phys. Rev.* **37**, 405 (1931).
12. L. Onsager, Reciprocal relations in irreversible processes. Part II. *Phys. Rev.* **38**, 2265 (1931).
13. E. O. Stejskal, J. E. Tanner, Spin diffusion measurements: spin echoes in the presence of time-dependent field gradient. *J. Chem. Phys.* **42**,

288–292 (1965).

14. E. O. Stejskal, Use of spin echoes in a pulsed magnetic-field gradient to study restricted diffusion and flow. *J. Chem. Phys.* **43**, 3597–3603 (1965).

15. P. J. Basser, J. Mattiello, D. L. Bihan, MR diffusion tensor spectroscopy and imaging. *Biophys. J.* **66**, 259–267 (1994).

16. P. J. Basser, C. Pierpaoli, Microstructural features measured using diffusion tensor imaging. *J. Magn. Reson.* **B**, 209–219 (1996).

17. P. J. Basser, J. Mattiello, D. LeBihan, Diagonal and off-diagonal components of the self-diffusion tensor: their relation to and estimation from the NMR spin-echo signal, *in* "Proc., SMRM, 11th Annual Meeting, Berlin, 1992," p. 1222.

18. J. Mattiello, P. J. Basser, D. LeBihan, Analytical expression for the b matrix in NMR diffusion imaging and spectroscopy. *J. Magn. Reson.* **A108**, 131–141 (1994).

19. D. Le Bihan, E. Breton, D. Lallemand, P. Grenier, E. Cabanis, M. Laval-Jeantet, MR imaging of intravoxel incoherent motions: application to diffusion and perfusion in neurologic disorders. *Radiology* **161**, 401–407 (1986).

20. P. J. Basser, J. Mattiello, D. Le Bihan, Estimation of the effective self-diffusion tensor from the NMR spin echo. *J. Magn. Reson* **B103**, 247–254 (1994).

21. P. J. Basser, J. Mattiello, R. Turner, D. L. Bihan, Diffusion *tensor* echo-planar imaging (DTEPI) of human brain, *in* "Proc., SMRM Workshop: Functional MRI of the Brain, Arlington, VA, 1993," p. 224.

22. M. K. Stehling, R. Turner, P. Mansfield, Echo-planar imaging: magnetic resonance imaging in a fraction of a second. *Science* **254**, 43–50

(1991).

23. R. J. Ordidge, J. A. Helpern, Z. X. Qing, R. A. Knight, V. Nagesh, Correction of motional artifacts in diffusion-weighted MR images using navigator echoes. *Magn. Reson. Imaging* **12**, 455–460 (1994).

24. P. Mansfield, I. L. Pykett, *J. Magn. Reson.* **29**, 355 (1978).

25. W. S. Price, P. W. Kuchel, Effect of nonrectangular field gradient pulses in the Stejskal and Tanner (diffusion) pulse sequence. *J. Magn. Reson.* **94**, 133–139 (1991).

26. M. Neeman, J. P. Freyer, L. O. Sillerud, Pulsed-gradient spin-echo studies in NMR imaging. Effects of the imaging gradients on the determination of diffusion coefficients. *J. Magn. Reson.* **90**, 303–312 (1990).

27. D. Le Bihan, Molecular diffusion nuclear magnetic resonance imaging. *Magn. Reson. Q,* **7**, 1–30 (1991).

28. D. Le Bihan, R. Turner, C. T. Moonen, J. Pekar, Imaging of diffusion and microcirculation with gradient sensitization: design, strategy, and significance. *J. Magn. Reson. Imaging* **1**:7–28 (1991).

29. J. H. Simpson, H. Y. Carr, Diffusion and nuclear spin relaxation in water. *Phys. Rev.* **111**, 1201–1202 (1958).

30. C. Pierpaoli, P. Jezzard, P. J. Basser, High-resolution diffusion tensor imaging of the human brain, *in* "SMR/ESMRMB Joint Meeting, Nice, 1995," p. 899.

31. L. Yang, T. H. Mareci, N. G. Harris, E. D. Wirth, B. A. Inglis, Diffusion tensor imaging of rat brain in vivo using a multiple stimulated echo sequence, *in* "Proc., SMR/ESMRMB Joint Meeting, Nice, 1995," p. 902.

Announcements of Meetings

Magnetic Resonance Imaging of the Brain, Spine and Musculoskeletal System, sponsored by the University of California, San Diego, School of Medicine, will be held on March 2–7, 1997, at the Hotel Del Coronado, Coronado California. This course is designed for physicians and allied health personnel and will cover the basic concepts of MR imaging and techniques, such as MR angiography, fat suppression MR imaging, and fast spin-echo sequences. Information from Ryals & Associates, Inc., P.O. Box 1925, Roswell, Georgia 30077-1925, tel (770) 641-9773, fax (770) 552-9859, email: Webmaster@Ryalsmeet.com, World Wide Web: http://www.ryalsmeet.com

4th Annual Update in General Diagnostic Imaging: Breast, Abdominal and Neuroradiology Imaging, sponsored by the University of Chicago, Department of Radiology, will be held on March 10–14, 1997, at the Breakers Resort Hotel, Palm Beach, Florida. This program will include a 4-hour mammography screening workshop, interventional breast procedures, screening for breast cancer, mammographic follow-up, imaging of cirrhosis, GU radiology, biliary disease, helical CT, interventional, transrectal and prostatic US, hydrocephalus, MS and white matter lesions, posterior fossa abnormalities. Information from Ryals & Associates, Inc., P.O. Box 1925, Roswell, Georgia 30077-1925, tel (770) 641-9773, fax (770) 552-9859, email: Webmaster@Ryalsmeet.com, World Wide Web: http://www.ryalsmeet.com

Minimally Invasive Therapy of the Brain, sponsored by the American Association of Physician Specialists, and the International Institute for Continuing Medical Education, will be held on March 14–16, 1997, at the Ritz-Carlton Hotel, Marina Del Rey, California. This 2½ day program is designed to provide neuroradiologists, neurologists, and radiologists with a special interest in minimally invasive therapy, a review of current approaches to brain tumors, vascular disease, and movement disorders using minimally invasive techniques. Information from Ryals & Associates, Inc., P.O. Box 1925, Roswell, Georgia 30077-1925, tel (770) 641-9773, fax (770) 552-9859, email: Webmaster@Ryalsmeet.com, World Wide Web: http://www.ryalsmeet.com